JACS Au
AN OPEN ACCESS JOURNAL OF THE AMERICAN CHEMICAL SOCIETY

pubs.acs.org/jacsau

Article

Variation of Tetrahydrofurans in Thyclotides Enhances Oligonucleotide Binding and Cellular Uptake of Peptide Nucleic Acids

Hongchao Zheng,[#] Victor Clausse,[#] Harsha Amarasekara, Sharlyn J. Mazur, Istvan Botos,* and Daniel H. Appella*

Cite This: *JACS Au* 2023, 3, 1952−1964

Read Online

ACCESS | Metrics & More | Article Recommendations | Supporting Information

ABSTRACT: Selective incorporation of conformational constraints into thyclotides can be used to modulate their binding to complementary oligonucleotides, increase polarity, and optimize uptake into HCT116 cells without assistance from moieties known to promote cell uptake. The X-ray structure and biophysical studies of a thyclotide−DNA duplex reveal that incorporation of tetrahydrofurans into an *aeg*PNA backbone promotes a helical conformation that enhances binding to complementary DNA and RNA. Selective incorporation of tetrahydrofurans into the *aeg*PNA backbone allows polarity to be increased incrementally so that uptake into HCT116 cells can be optimized. The enhanced binding, polarity, and cellular uptake properties of thyclotides were used to demonstrate effective inhibition of microRNA-21 in HCT116 cells.

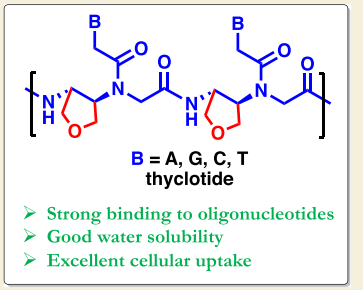

KEYWORDS: *thyclotide, peptide nucleic acids (PNAs), binding properties, cell uptake, X-ray crystal structure, backbone modification, miR-21 inhibition, preorganization*

INTRODUCTION

Since the 1980s, scientists have worked to develop chemically modified oligonucleotides with antisense sequences that can alter gene expression by binding to DNA or RNA target sequences within cells. Despite the potential for antisense molecules to be developed as drugs, only a few have been approved for clinical use.[1−4] In 1991, Nielsen and co-workers first described the nucleic acid analogues termed peptide nucleic acids (PNAs) (Figure 1).[5−9] The most common PNA (**1**) consists of nucleobases bonded to a highly flexible *N*-(2-aminoethyl) glycine (*aeg*) backbone that does not occur naturally. The lack of negative charge on the pseudopeptide backbone of *aeg*PNA **1** facilitates strong binding to complementary oligonucleotides, and the synthetic backbone conveys resistance to enzymatic degradation.[10−14] These unique properties make *aeg*PNAs ideal molecules for antisense applications in addition to probes for molecular diagnostics.[15−24] However, *aeg*PNAs are limited by poor cellular uptake and low aqueous solubility.[25] Numerous efforts have been made to modify *aeg*PNA to address these concerns,[26−31] and the addition of charged groups either to the backbone or the ends of *aeg*PNA will improve aqueous solubility and cellular uptake *via* mechanisms typically involving endocytosis. In general, *aeg*PNA needs the assistance of a delivery mechanism to enter cells, and there are many strategies available with varying degrees of success.[32−36] In our previous work, we have shown that cyclopentane (*cp*) groups incorporated into the *aeg*PNA backbone constrain the flexible *aeg* backbone to adopt a right-handed helical conformation with improved binding affinity to complementary nucleic acids (Figure 1, *cp*PNA **2**).[37] The hydrophobic *cp* rings on the backbone, however, do not improve water solubility. We reasoned that the introduction of a more polar five-membered ring, tetrahydrofuran (*thf*), into the PNA backbone could potentially improve its water solubility while maintaining the binding properties of *cp*PNA (Figure 1). In this article, we present detailed insights into the chemical, biophysical, structural, and biological properties of tetrahydrofuran-derived PNAs **3** (which we call thyclotides). We previously demonstrated that thyclotides containing *thf* at every position in a PNA sequence could enter cells and target a microRNA sequence.[38] Here, we show how the incremental incorporation of *thf* groups into a PNA sequence affects binding to oligonucleotides and leads to additional improvements in cellular uptake. Compared with *aeg*PNA, thyclotides display stronger binding affinity to complementary DNA and RNA. While placing *thf* at every position in a PNA sequence that targets microRNA-21 resulted in good cellular uptake,[38] we show in this article that careful placement of *thf* groups at only select positions results in more favorable cell uptake and

Received: April 19, 2023
Revised: June 15, 2023
Accepted: June 16, 2023
Published: June 29, 2023

https://doi.org/10.1021/jacsau.3c00198
JACS Au 2023, 3, 1952−1964

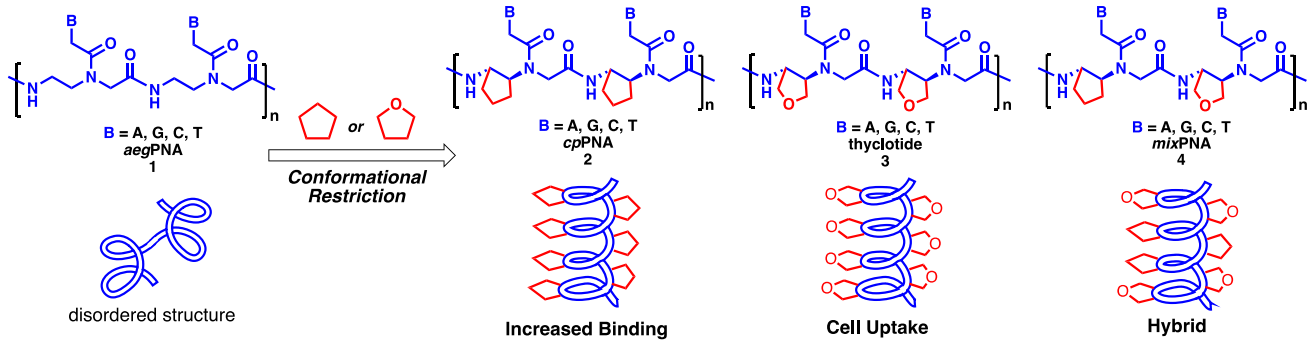

Figure 1. Approaches to controlling the backbone conformations of *aeg*PNAs by incorporation of cyclopentanes or tetrahydrofurans.

Table 1. *aeg*PNA, Thyclotide, and *cp*PNA Used in the Melting Experiments

PNA[a]	sequence	number (*aeg*PNA residue)	number (*thf*PNA residue)	number (*cp*PNA residue)
*aeg*PNA **1a**	GATGTGATA	9	0	0
thyclotide **3a**	GATGT*GATA	8	1	0
thyclotide **3b**	GAT*GTGAT*A	7	2	0
thyclotide **3c**	GAT*GT*GAT*A	6	3	0
thyclotide **3d**	GA*T*GT*GAT*A	5	4	0
thyclotide **3e**	GA*T*GT*GA*T*A	4	5	0
thyclotide **3f**	GA*T*GT*GA*T*A*	3	6	0
thyclotide **3g**	G*A*T*GT*GA*T*A*	2	7	0
thyclotide **3h**	G*A*T*G*T*GA*T*A*	1	8	0
thyclotide **3i**	G*A*T*G*T*G*A*T*A*	0	9	0
*mix*PNA **4a**	G*A*T*G#T#G#A*T*A*	0	6	3
*cp*PNA **2a**[37]	G#A#T#G#T#G#A#T#A#	0	0	9

[a]Cyclopentane stereochemistry is (*S*,*S*), and tetrahydrofuran stereochemistry is (*R*,*R*); B* = *thf* residue, B# = *cp* residue. PNA and thyclotide sequences are written from the N- to C-terminal. In each oligomer, 2-aminoethoxy-2-ethoxy acetic acid (AEEA) is the first residue at the C-terminal, and the N-terminal is a free amine.

enhanced biological activity against the microRNA target. We also show that both *cp* and *thf* groups may be incorporated into a *mix*PNA **4**. The unique properties of thyclotides may provide a new strategy for the cellular delivery of antisense molecules.

RESULTS AND DISCUSSION

Preparation of Thyclotides

Thyclotide oligomers are prepared from monomers using Fmoc-based solid phase peptide synthesis (SPPS). An efficient synthetic route for the preparation of thyclotide monomers was developed based on the protocols for *cp*PNA monomers.[38] Initially, a nine-residue mixed-base sequence was chosen to study the properties of the thyclotides. Using this test sequence, *thf* groups were gradually introduced into the sequence.[37] Nine different thyclotides **3a**−**3i**, one *cp*PNA **2a**, and one mixed PNA **4a** were prepared (Table 1).

In each oligomer, 2-aminoethoxy-2-ethoxy acetic acid (AEEA) is the first *C*-terminal residue and the *N*-terminal is a free amine. After the completion of peptide synthesis, the oligomer is cleaved from the resin, all protecting groups are removed, and the crude products are purified by reversed-phase high-pressure liquid chromatography (RP-HPLC) (Figure 2A,B, Figures S53−S107, and Tables S17−S19). Before subsequent studies, each oligomer is characterized by ESI-TOF mass spectrometry (Table S1 and Figures S53−S107).

Polarity and Single-Strand Circular Dichroism (CD)

The relative polarities of *aeg*PNA **1a**, *cp*PNA **2a**, thyclotide **3i**, and *mix*PNA **4a** were examined by RP-HPLC outfitted with a C18 column while eluting with a mixture of water and acetonitrile. The retention time of a molecule on the C18 column is related to the polarity and hydrophobicity of the molecule. The HPLC chromatogram of a mixture of **1a**, **2a**, **3i**, and **4a** showed that thyclotide **3i** elutes first, followed by *aeg*PNA **1a**, *mix*PNA **4a**, and finally, *cp*PNA **2a** (Figure 2A,B). This observation indicates that the thyclotide is more polar than *aeg*PNA and *cp*PNA.

According to the "like dissolves like" rule,[39] the increase in polarity of the thyclotide leads to its enhanced solubility in water compared with *aeg*PNA and *cp*PNA. The *mix*PNA with three *cp* and six *thf* groups elutes later than the *aeg*PNA, indicating that the *cp* groups contribute significant hydrophobicity to the molecule. The relative hydrophilicity was further assessed by determining distribution of each molecule at equilibrium between octanol and water. Within the series, thyclotide **3i** has the lowest octanol/water partition coefficient ($K_{ow} = 2.59 \times 10^{-3}$) and, therefore, a higher affinity for the aqueous phase than *aeg*PNA **1a** ($K_{ow} = 5.03 \times 10^{-3}$), *mix*PNA **4a** ($K_{ow} = 1.85 \times 10^{-2}$), and *cp*PNA **2a** ($K_{ow} = 4.58 \times 10^{-2}$; Table S2 and Figures S1−S8). The circular dichroism (CD) spectra of *aeg*PNA **1a**, thyclotide **3i**, *mix*PNA **4a**, and *cp*PNA **2a** were each measured in water (Figure 2C). Except for **1a**, each molecule reveals a

https://doi.org/10.1021/jacsau.3c00198
JACS Au 2023, 3, 1952−1964

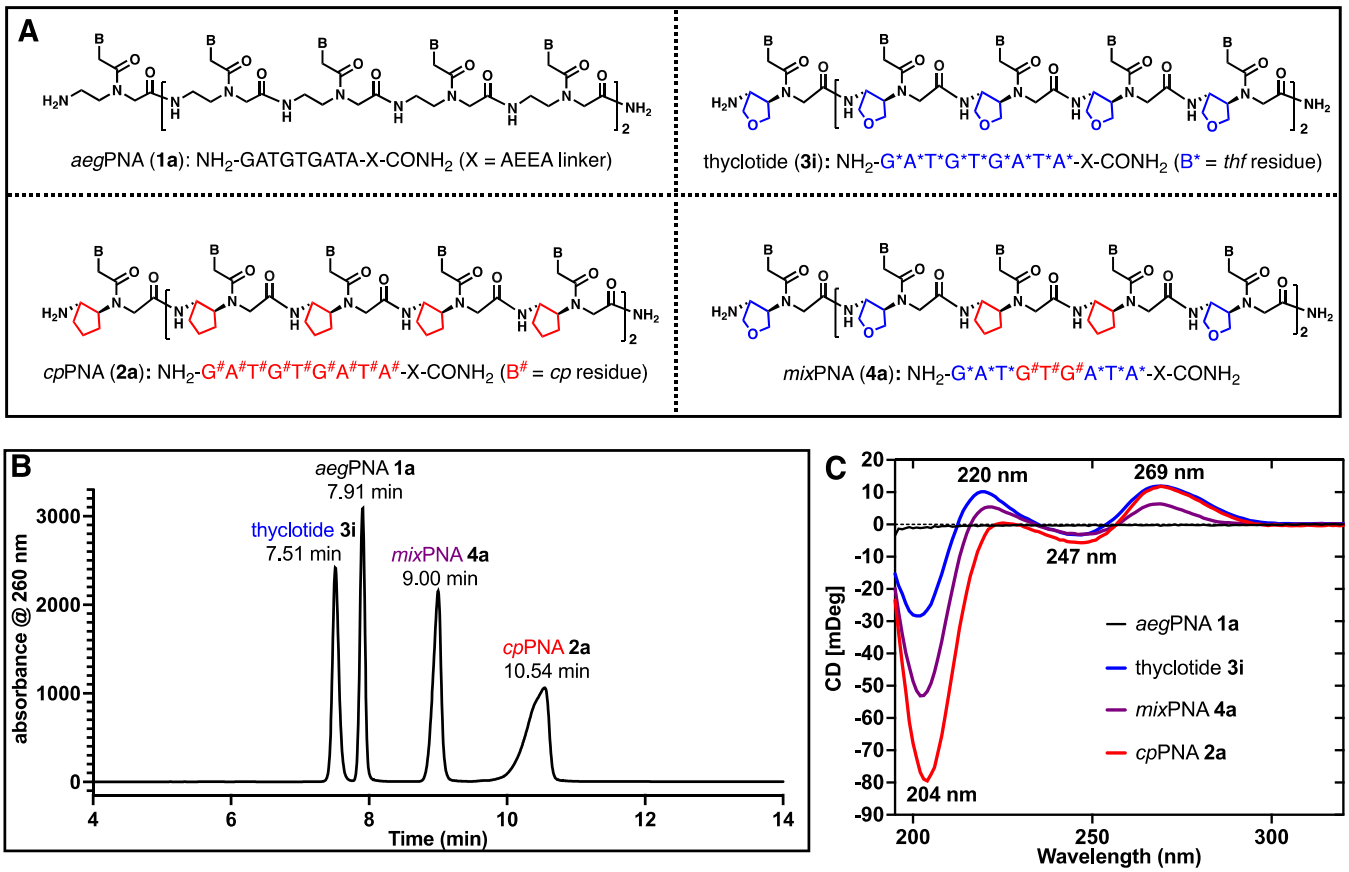

Figure 2. Backbone modifications of peptide nucleic acids (PNAs) with tetrahydrofuran (*thf*) and cyclopentane (*cp*). (A) Structural schematic of *aeg*PNA (top left), thyclotide (top right), *cp*PNA (bottom left), and *mix*PNA (bottom right). Nine-nucleobase sequences representing *aeg*PNA **1a**, thyclotide **3i**, *cp*PNA **2a**, and *mix*PNA **4a**. B* represents *thf* residue, B$^{\#}$ represents *cp* residue, and AEEA = 2-(2-aminoethoxy)ethoxyacetyl group. (B) HPLC chromatogram of a mixture of *aeg*PNA **1a**, *cp*PNA **2a**, thyclotide **3i**, and *mix*PNA **4a** (~1:1:1:1 ratio). (C) CD spectra of unhybridized (single-strand) *aeg*PNA **1a**, thyclotide **3i**, *cp*PNA **2a**,[37] and *mix*PNA **4a** (50 μM in water).

distinct CD spectrum that will be discussed in a subsequent section.

UV Experiments

The effects of *thf* substitution on the binding of thyclotides to DNA and RNA were determined by examining the melting temperatures (T_m's) for molecules **3a**−**3i** and comparing the change (ΔT_m) relative to unmodified *aeg*PNA **1a** (Figure 3A,B, Figures S9−S14, and Table S3). Our results show that a single *thf* in a thyclotide increases the melting temperature of the duplex with complementary DNA as well as RNA (**1a** *vs* **3a**, Figure 3A,B). Additional *thf* units further increase the T_m values (**3b**−**3i**). The average increase in T_m per *thf* modification is around +4 °C for DNA binding and +3 °C for RNA binding. When bound to DNA, the fully *thf*-modified thyclotide **3i** has a T_m of 77 °C, an increase of 35 °C compared to the corresponding *aeg*PNA−DNA duplex. When bound to RNA, thyclotide **3i** has a T_m of 72 °C, which is 26 °C higher than that of the corresponding *aeg*PNA−RNA duplex (**1a** *vs* **3i**, Figure 3A,B). For thyclotides **3a**−**3e**, which contain one to five *thf* groups, the T_m values of the thyclotide−RNA duplexes are higher than the corresponding thyclotide−DNA duplexes (Figure 3A,B). This observation is consistent with *aeg*PNA, which typically shows higher T_m values when bound to RNA versus DNA. When additional five-membered rings are incorporated in the backbone, as with thyclotides **3f**−**3i**, *mix*PNA **4a**, and *cp*PNA **2a**, the T_m values for DNA binding are higher than for RNA binding (Figure 3A,B). The increase in duplex stability with DNA associated with several five-membered rings in the PNA backbone may indicate that the RNA backbone, which is more rigid than DNA, is less able to accommodate the increases in PNA rigidity as additional five-membered rings are introduced. Interestingly, the stabilizing effect of *thf* for the PNA−DNA and RNA duplexes is lower than that of *cp* (**3i** *vs* **4a** and **2a**, Figure 3A,B). Because *cp* and *thf* rings have very similar conformations,[40] we were surprised by this noticeable difference in the T_m values of *cp*PNA−DNA and RNA duplexes compared with the thyclotide duplexes of identical sequences. Combining *cp* and *thf* groups in the *mix*PNA **4a** showed T_m values of 85 °C for DNA binding and 80 °C for RNA binding, which are higher than that of the fully *thf*-modified thyclotide **3i**. The observation that *cp* groups continued to provide improved duplex stability compared with *thf* even in *mix*PNA **4a** prompted us to further characterize the properties of thyclotides.

The ability of a PNA to discriminate between fully complementary DNA or RNA sequences versus similar sequences with only a one base mismatch is defined as the sequence specificity. In these experiments, the T_m of a duplex containing a single base mismatch is subtracted from the T_m of a duplex of the fully matched duplex to provide a ΔT_m value. Larger ΔT_m values indicate a higher degree of sequence specificity. The ΔT_m of thyclotide **3i** is greater than that of the corresponding *aeg*PNA **1a** and comparable to those of *cp*PNA **2a**

https://doi.org/10.1021/jacsau.3c00198
JACS Au 2023, 3, 1952−1964

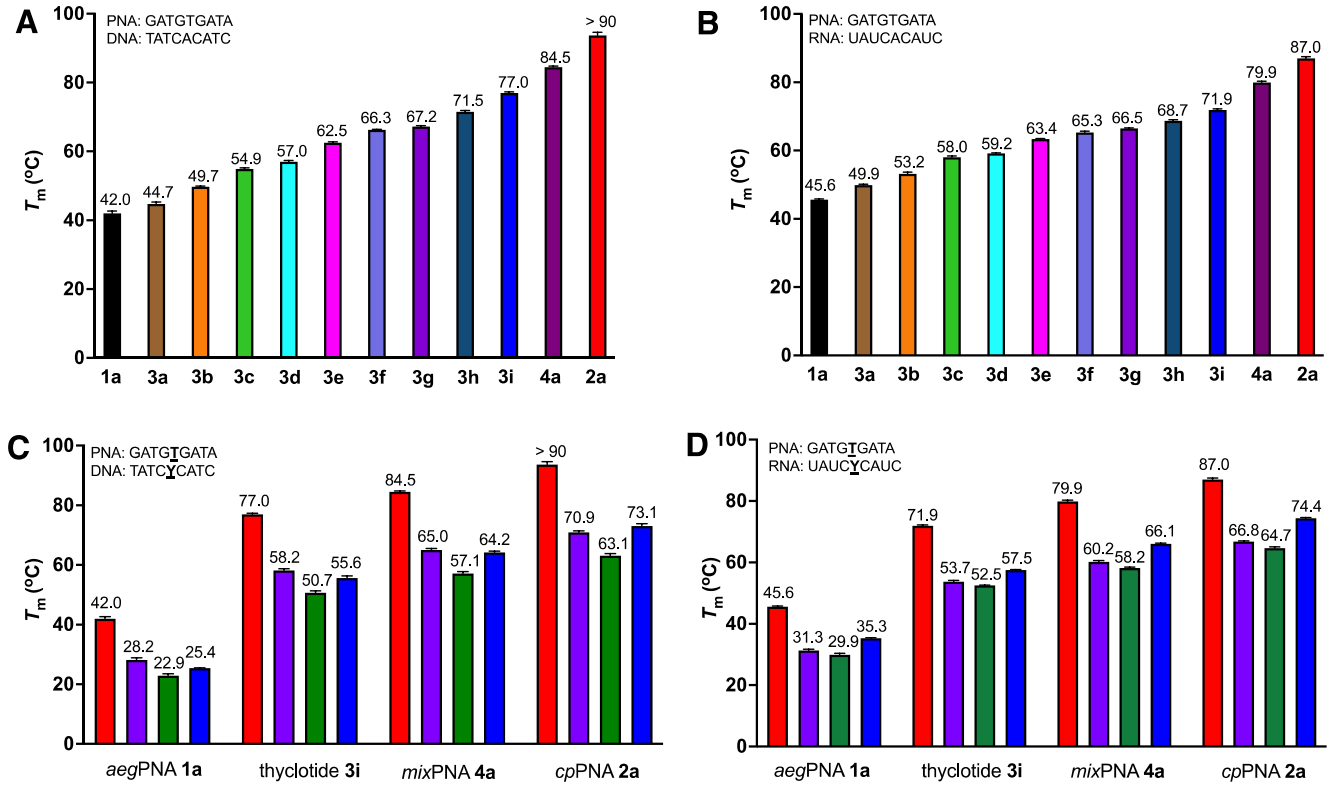

Figure 3. Thyclotide exhibits strong binding properties to oligonucleotides. (A) Melting temperatures for PNA−DNA duplexes (1 μM individual strand concentration) in PBS. (B) Melting temperature data for PNA−RNA duplexes (1 μM individual strand concentration) in PBS. (C) Comparison of single base mismatch discrimination between *aeg*PNA, thyclotide, and *cp*PNA for DNA binding. Color codes for Y in the DNA strand: A (red), T (purple), C (green), and G (blue). (D) Comparison of single base mismatch discrimination between *aeg*PNA, thyclotide, and *cp*PNA for RNA binding. Color codes for Y in the RNA strand: A (red), U (purple), C (green), and G (blue).

and *mix*PNA **4a** (Figure 3C,D, Figures S15−S26, and Tables S4 and S5). The thyclotide **3i**, *cp*PNA **2a**, and *mix*PNA **4a** displayed better sequence specificity for DNA binding than RNA binding when comparing ΔT_m values (Figure 3C *vs* Figure 3D). When binding to the DNA or RNA with a TT mismatch or a TC mismatch, thyclotide **3i** exhibited slightly worse sequence specificity than *cp*PNA **2a** and *mix*PNA **4a**. In contrast, when binding to the DNA or RNA with a TG mismatch, thyclotide **3i** showed slightly better sequence fidelity than *cp*PNA **2a** and *mix*PNA **4a**. Despite some minor differences, the improvements in the sequence specificity of *cp* and *thf* groups in a PNA backbone are about the same.

Thermodynamic Analysis

To better understand the contribution of *thf* to the stability of the PNA−DNA or RNA duplex, nonlinear least-squares curve fitting[41] was used to analyze the UV melting curves to determine the thermodynamic parameters for *aeg*PNA **1a**, thyclotides **3a**−**3i**, *mix*PNA **4a**, and *cp*PNA **2a** for hybridization to DNA or RNA. The data are listed in Tables S6 and S7. Our results show that the binding constant consistently increases as more *thf* units are introduced into the PNA backbone (**1a** *vs* **3a**−**3i**, Tables S6 and S7). Compared with the unmodified *aeg*PNA **1a**, the binding affinity to DNA and RNA for fully modified thyclotide **3i** is increased by five orders of magnitude and four orders of magnitude, respectively. The binding of PNAs to complementary oligonucleotides is typically driven by favorable enthalpy resulting from hydrogen bonding between nucleobases that overcomes unfavorable entropy resulting from the loss of conformational freedom of the free PNA and the oligonucleotide when forming a duplex structure. As the number of *thf* groups is gradually increased for thyclotides **3a**−**3h**, the binding to DNA mostly improves as a result of less unfavorable entropy compared with *aeg*PNA **1a**. The increase in binding affinity for *cp*PNA **2a** for DNA is also largely driven by less unfavorable entropy (Table S6). This observation could be an effect of the conformational rigidification of the backbone with *thf*. However, the increased binding affinities for thyclotide **3i** and *mix*PNA **4a** binding to DNA are enthalpically driven (Table S6), as are the RNA binding of thyclotides **3a**−**3i**, *mix*PNA **4a**, and *cp*PNA **2a** (Table S7). Clearly, the binding of thyclotides and *cp*PNA to DNA and RNA is governed by a complex interplay of enthalpy and entropy compensation.[42] However, the thymodynamic data do not reveal an explanation for why thyclotides bind with slightly weaker affinity to oligonucleotides compared to *cp*PNA.

Circular Dichroism (CD)

To determine the effect of *thf* on the helical conformation of PNA, we measured the CD spectra of thyclotides **3a**−**3i**. The *aeg*PNA **1a** lacks any distinct peaks because it is achiral and has an unstructured non-helical conformation.[43] For thyclotides **3a**−**3i**, we observed positive peaks around 220 and 269 nm and negative peaks around 204 and 247 nm (Figure S39). These CD signals suggest that thyclotides adopt a right-handed helical conformation that is intermediate between A- and B-form DNA (Figure S39).[44] The magnitude of the CD signals increases as more *thf* groups are present in the PNA backbone. However, thyclotide **3i** exhibits a much weaker CD signal compared to *mix*PNA **4a** and *cp*PNA **2a** (Figure 2C), suggesting that it has a lower degree of helicity. The incorporation of polar side chains

https://doi.org/10.1021/jacsau.3c00198
JACS Au 2023, 3, 1952−1964

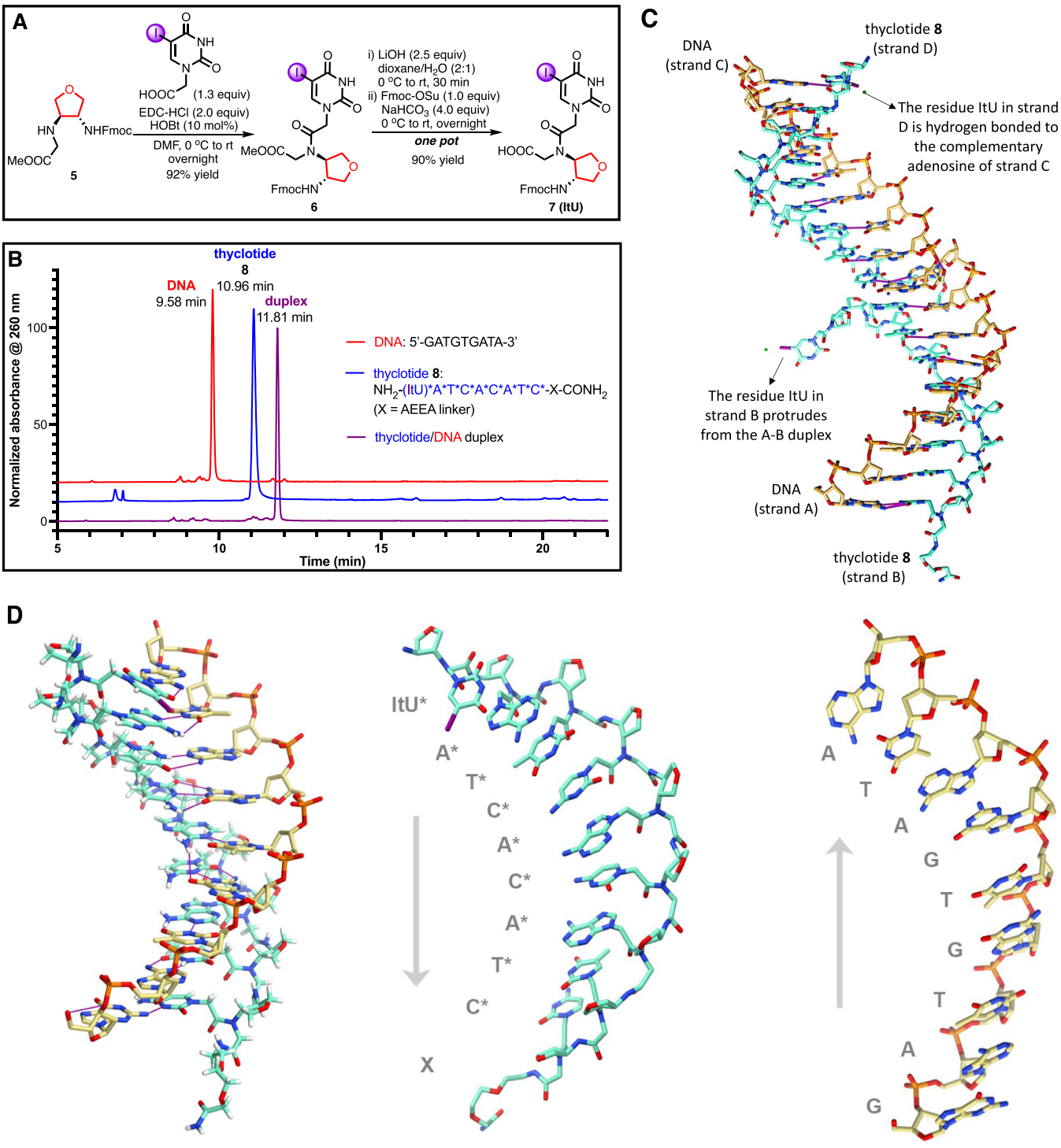

Figure 4. Synthesis, purification, and crystal structure of iodo-labeled thyclotide **8** with complementary DNA. (A) Synthetic route for the preparation of iodo-labeled thyclotide monomer **7**. (B) HPLC chromatograms of iodo-labeled thyclotide **8** (blue), its complementary DNA (red), and thyclotide **8**−DNA duplex (purple). ItU* represents iodo-labeled thyclotide residue **7**, B* represents *thf* residue, and X represents 2-aminoethoxy-2-ethoxy acetic acid (AEEA linker). (C) Stick view of thyclotide **8**−DNA double-helix (two helices, A−B duplex and C−D duplex, in the asymmetric crystallographic unit). Hydrogen bonds are shown as purple lines. (D) Stick views of thyclotide **8**−DNA double-helix structure (C−D duplex, left), the iodo-labeled thyclotide **8** (strand D, middle), and its complementary DNA (strand C, right). Resolution = 2.0 Å, R/R_{free} = 23.2/26.4, and space group = *I*222. Hydrogen bonds are shown as purple lines.

in α-helical polypeptides may similarly lower the α-helical stability in aqueous solution by decreasing hydrophobic interactions.[45,46] The change from hydrophobic cyclopentane groups to more polar *thf* groups in the PNA backbone also seems to elicit a decrease in helical stability for thyclotide **3i**. The CD data are consistent with our observations that the average increase in T_m per *cp* modification is around +6 °C for DNA binding and +4.5 °C for RNA binding, whereas the average increase in T_m per *thf* modification is around +4 °C for DNA binding and +3 °C for RNA binding. The magnitudes of CD

https://doi.org/10.1021/jacsau.3c00198
JACS Au 2023, 3, 1952−1964

Table 2. Comparison of Helical Parameters between Available PNA−DNA and Thyclotide−DNA Complexes[a]

structure	type	twist [°]	rise [Å]	base tilt [°]	displacement [Å]	bases per turn	method
7UID (A−B)	thyclotide−DNA	22.5	3.3	1.6	−5.3	16.0	X-ray
7UID (C−D)	thyclotide−DNA	24.3	3.3	1.4	−5.4	14.8	X-ray
7KZL	*cp*PNA−DNA[37]	27.1	3.4	0.4	−3.4	13.2	X-ray
1PDT	PNA−DNA[50]	27.5	3.5	−1.3	−2.9	13.1	NMR
3PA0	*γ*PNA−DNA[51]	22.6	3.3	3.0	−6.6	15.9	X-ray
1NR8	*α*PNA−DNA[52]	23.0	3.4	0.7	−4.2	15.7	X-ray
A-DNA	DNA−DNA[53]	32.7	2.6	−4.5	−4.5	11	X-ray
B-DNA	DNA−DNA[53]	36.0	3.4	−0.1	0.0	10	X-ray

[a]A−B and C−D refer to the two duplexes in the asymmetric crystallographic unit from this work. One duplex is the pairing of strands A and B, and the other is the pairing of strands C and D. The averaged values were calculated with CURVES.[48]

signals for thyclotides are smaller than those of *mix*PNA **4a** and *cp*PNA **2a**, yet these CD data suggest that the *thf* modification preorganizes the backbone of PNAs into a right-handed helix to some degree. The helical preorganization most likely accounts for their enhanced binding affinity to the complementary DNA or RNA.

Preparation and Purification of the Iodo-Labeled Thyclotide−DNA Duplex

Thyclotides exhibit increased binding affinity to DNA and are more polar compared with *aeg*PNA, yet the binding affinity of *cp*PNA to DNA is considerably stronger than the corresponding thyclotide. One potential explanation of this difference in binding affinity is that the *thf* groups sterically interfere with binding due to slight differences in the conformations of the five-membered ring. To gain insight into this possibility, an X-ray structure of a thyclotide−DNA duplex was determined to observe the orientations of the *thf* groups. For these studies, either the thyclotide or the DNA must be labeled with a heavy atom such as iodide atom to solve the phase problem that is encountered in X-ray crystallography.[47] Duplexes of thyclotides with commercially available iodo-labeled DNAs did not yield good quality crystals. Therefore, a synthesis for iodo-labeled thyclotide was developed. Monomer **7** was prepared following a similar procedure for the preparation of the other thyclotide monomers.[38] The Fmoc-protected tetrahydrofuran diamine **5** was coupled with 5-iodouracil-1-yl acetic acid using *N*-ethyl-*N*′-(3-dimethylaminopropyl)carbodiimide hydrochloride (EDC) and hydroxybenzotriazole (HOBt) to afford the iodo-labeled thyclotide monomer methyl ester derivative **6**. The resulting methyl ester was subjected to ester hydrolysis, followed by Fmoc protection to yield the requisite iodo-labeled thyclotide monomer **7** (Figure 4A and Scheme S1). The iodo-labeled thyclotide monomer **7** is compatible with standard Fmoc-based solid-phase synthesis, and a 9-mer thyclotide bearing a 5-iodouridine residue at the terminal position **8** was thus prepared (Figure 4B). HPLC was used to monitor the formation of the thyclotide−DNA duplex (see page S25 for details). When the iodo-labeled thyclotide **8** was mixed with its complementary DNA in a 1:1 ratio in water at room temperature, the duplex was formed exclusively (Figure 4B). The duplex was successfully purified by HPLC as the duplex peak is well separated from free thyclotide and free DNA on the HPLC chromatogram. The purified iodo-labeled thyclotide **8**−DNA duplex formed single crystals used for X-ray diffraction analysis.

X-ray Diffraction Analysis of the Thyclotide−DNA Duplex

The structure of the duplex was solved by single-wavelength anomalous diffraction phasing using the iodo-labeled thyclotide **8** at 2.0 Å resolution in the space group *I*222 and refined to an R_{factor} of 23.2% and an R_{free} of 26.4% (Table S8 and Figures S40−S48). Two helices, the A−B duplex and C−D duplex, were identified in the asymmetric unit (Figure 4C and Figures S49 and S50). In the C−D helix, all nucleobases on thyclotide **8** (strand D) are hydrogen-bonded to the nucleobases on its complementary DNA strand (strand C). In the A−B helix, the iodo-uridine residue on thyclotide **8** (strand B) is flipped out of the A−B duplex. Its complementary nucleobase, an A residue at the end of the complementary DNA strand (strand A), seems to interact with a G nucleobase of strand C in the C−D helix (possibly through hydrogen bonding). Although the sterically hindered iodine atom in the iodo-uridine nucleobase might weaken its hydrogen bonding to the complementary nucleobase, the flipped-out conformation of the iodo-uridine nucleobase is likely a result of crystal packing. The helical parameters of the two duplexes in the asymmetric unit are slightly different. The thyclotide **8**−DNA A−B helix (A−B duplex with the flipped-out iodo-uridine) forms an antiparallel right-handed helix with a helical twist of 22.5 Å, a rise of 3.3 Å, and a pitch of 16.0 base pairs per turn (Figure 4C, Tables S9 and S11, and Table 2 (7UID: A−B)). The fully base-paired C−D duplex adopts a more twisted right-handed helix with a helical twist of 24.3 Å, a rise of 3.3 Å, and a pitch of 14.8 base pairs per turn (Figure 4D, Tables S10 and S12, and Table 2 (7UID: C−D)). In the structure of the C−D duplex, all nucleobases pair *via* Watson−Crick hydrogen bonds and the base pairs are almost perpendicular to the helical axis (Figure 4D). Both the *thf* units and the carbonyl groups of the peptide backbone orient toward the solvent, while the carbonyl in the carboxymethyl groups next to the nucleobases points toward the C-terminal. Taken together, the thyclotide−DNA duplex adopts a P-form helix (Figure 4D and Table 2).[49] The thyclotide−DNA duplex exhibits a slightly smaller twist angle than the *cp*PNA−DNA duplex (entries 2 and 3, Table 2) and larger twist angles than other backbone-modified PNA−DNA duplexes (entries 5 and 6, Table 2).[37,50−53] The helical parameters suggest that the thyclotide−DNA duplex adopts a P-form helical structure that resembles the *cp*PNA−DNA duplex. Overall, the thyclotide−DNA structure demonstrates that *thf* is a good backbone-rigidifying unit that is nicely accommodated in the complex with DNA.

Cyclopentane and tetrahydrofuran have very similar envelope conformations,[40] and both are well tolerated in the structures of *cp*PNA and thyclotide when bound to DNA. Therefore, it is unlikely that conformational differences between the two rings would explain why a thyclotide−DNA duplex exhibits lower thermodynamic stability than the corresponding *cp*PNA−DNA duplex. After superimposing the two X-ray structures, we observed a substantial difference in the number of water

https://doi.org/10.1021/jacsau.3c00198
JACS Au 2023, 3, 1952−1964

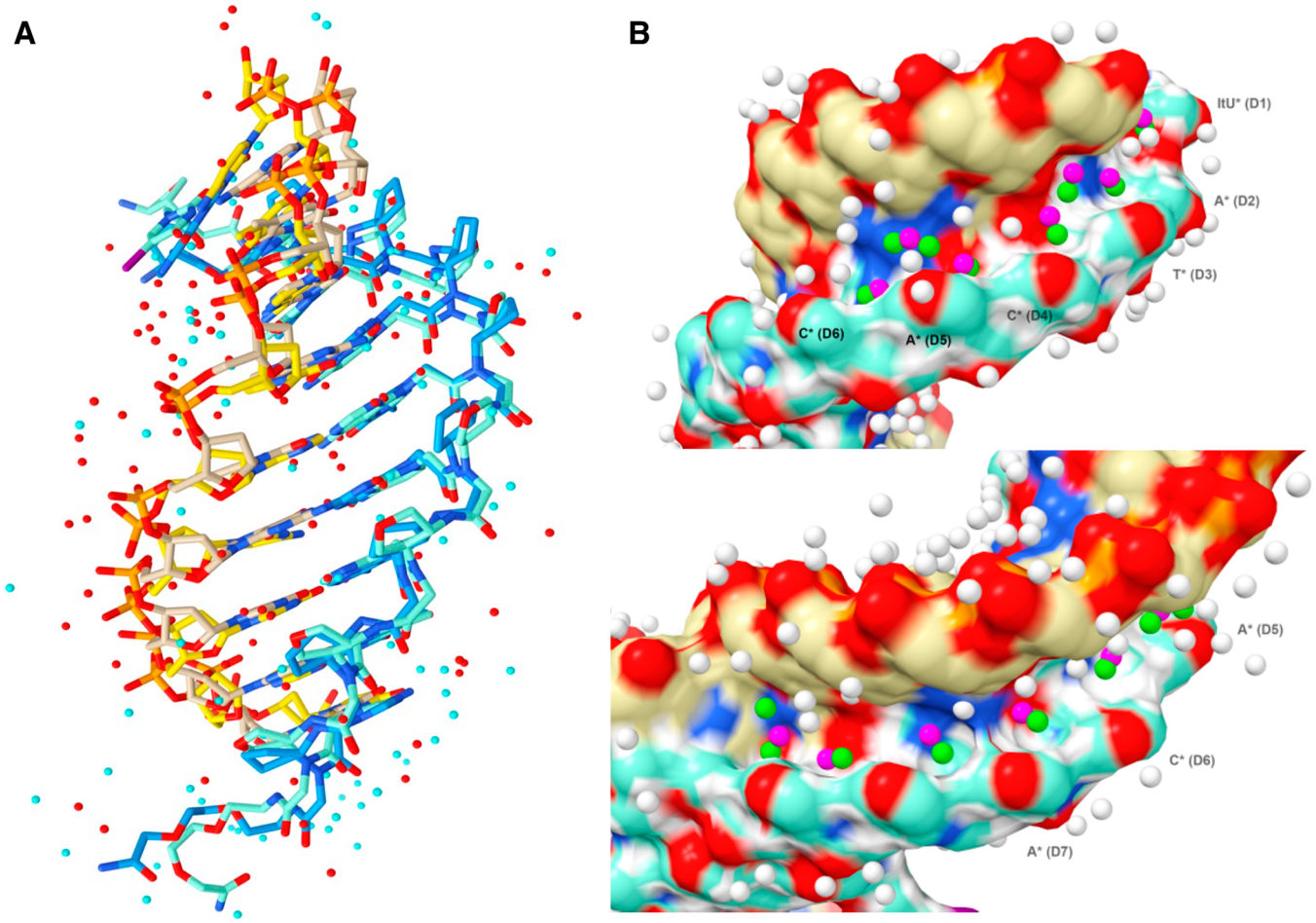

Figure 5. The thyclotide **8**−DNA duplex has more water molecules than the *cp*PNA **2a**−DNA duplex (PDB: 7KZL). (A) Superimposed stick views of *cp*PNA **2a**−DNA (PDB: 7KZL)[37] and thyclotide **8**−DNA (PDB: 7UID) duplexes with water molecules from both structures. Color scheme for PNAs and DNA: *cp*PNA **2a** is dark blue, DNA bound to *cp*PNA **2a** is yellow, thyclotide **8** is cyan, and DNA bound to thyclotide **8** is khaki. Color scheme for water molecules: cyan spheres are water molecules from the thyclotide **8**−DNA duplex, and red spheres are water molecules from the *cp*PNA **2a**−DNA duplex. (B) Two surface views of the thyclotide **8**−DNA duplex. Color scheme for PNA and DNA: thyclotide **8** is cyan, and DNA is khaki. Color scheme for water molecules: green spheres represent conserved water molecules observed only in the thyclotide **8**−DNA duplex, magenta spheres represent conserved water molecules seen only in the *cp*PNA **2a**−DNA duplex, and white spheres represent non-conserved water molecules observed in both the thyclotide **8**−DNA and *cp*PNA **2a**−DNA duplexes. ItU* represents iodo-labeled thyclotide residue **7**, and B* represents *thf* residue.

Table 3. Values of Δn_w (per Base Pair)[a]

PNA[a]	sequence	Δn_w (ethylene glycol)	Δn_w (glycerol)
thyclotide **9a** (with DNA)	T*G*T*G*A*T*A*	0.72 ± 0.03	0.92 ± 0.03
*cp*PNA **9b** (with DNA)	$T^{\#}G^{\#}T^{\#}G^{\#}A^{\#}T^{\#}A^{\#}$	0.47 ± 0.01	0.74 ± 0.03
thyclotide **9a** (with RNA)	T*G*T*G*A*T*A*	0.95 ± 0.03	1.16 ± 0.04
*cp*PNA **9b** (with RNA)	$T^{\#}G^{\#}T^{\#}G^{\#}A^{\#}T^{\#}A^{\#}$	0.76 ± 0.03	0.87 ± 0.03

[a]Cyclopentane stereochemistry is (*S*,*S*), and tetrahydrofuran stereochemistry is (*R*,*R*); B* = *thf* residue, and $B^{\#}$ = *cp* residue. PNA and thyclotide sequences are written from the N- to C-terminal. In each oligomer, 2-aminoethoxy-2-ethoxy acetic acid (AEEA) is the first residue at the C-terminal, and the N-terminal is a free amine.

molecules surrounding the helices. There are around 97 water molecules identified in the *cp*PNA−DNA duplex and 156 water molecules in the thyclotide−DNA duplex (Figure 5A,B). It is important to note that the *cp*PNA−DNA duplex was solved at 1.3 Å resolution, whereas the thyclotide−DNA duplex was solved at 2.0 Å resolution. Furthermore, water molecules are identified more readily in structures with 1.0 Å resolution compared to those solved at 2.0 Å resolution.[54] The fact that many additional water molecules were identified in the structure of the thyclotide−DNA at 2.0 Å resolution compared to the *cp*PNA−DNA at 1.3 Å resolution indicates that thyclotides are more extensively hydrated than *cp*PNA. The increased hydration of thyclotides in aqueous solutions may explain the lower thermodynamic stability of thyclotide−DNA duplexes compared with *cp*PNA−DNA duplexes, as well as the weaker CD signals.[55]

https://doi.org/10.1021/jacsau.3c00198
JACS Au 2023, 3, 1952−1964

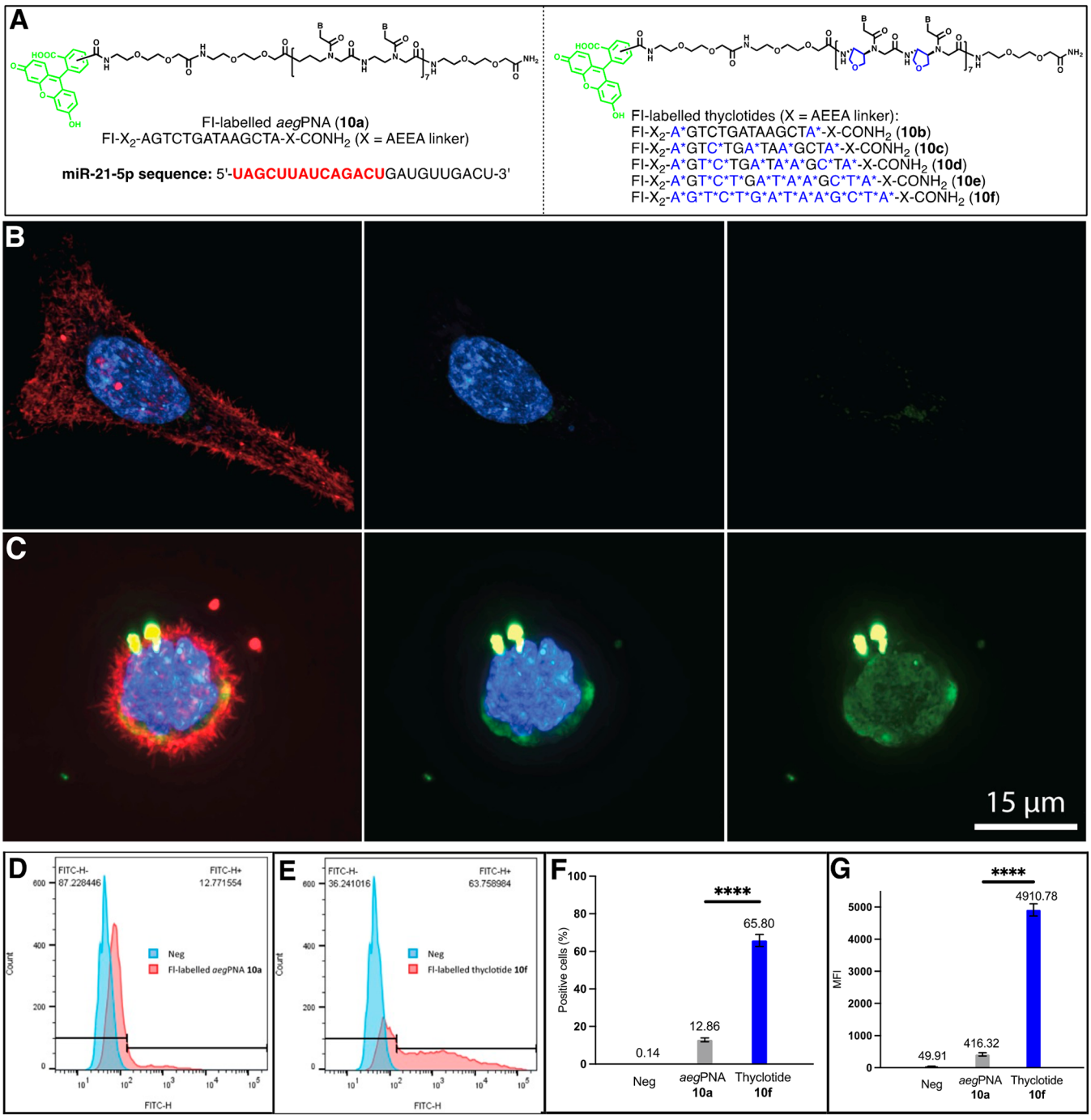

Figure 6. Thyclotide exhibits cell uptake enhancement compared with *aeg*PNA. (A) Schematic of the fluorescein-labeled (Fl) *aeg*PNA **10a** and fluorescein-labeled thyclotide **10b**−**10f** used in cell uptake experiments. B* represents *thf* residue, and X represents 2-aminoethoxy-2-ethoxy acetic acid (AEEA linker). (B) 3D volume reconstruction of 0.15 μm z-steps super-resolution microscopy of an HCT116 cell treated with 2.5 μM **10a** for 3 h. The cell was stained with the Membrite Fix 640/660 membrane marker and Hoechst 33342 for nucleus staining. The membrane (red) and nucleus (blue) channels were successively removed from the middle and right pictures, respectively, to better show the cytoplasmic and nuclear diffusion of the *aeg*PNA **10a** (green). (C) 3D volume reconstruction of 0.15 μm z-steps super-resolution microscopy of an HCT116 cell treated with 2.5 μM **10f** for 3 h. The cell was stained with the Membrite Fix 640/660 membrane marker and Hoechst 33342 for nucleus staining. The membrane (red) and nucleus (blue) channel were successively removed from the middle and right pictures, respectively, to better show the cytoplasmic and nuclear diffusion of the thyclotide **10f** (green). (D) FACS data of HCT116 comparing the fluorescence of cells not treated or treated with **10a** for 3 h. (E) FACS data of HCT116 comparing the fluorescence of cells not treated or treated with **10f** for 3 h. (F) Mean of fluorescence intensity for negative control, *aeg*PNA-treated cells, and thyclotide-treated cells. (G) FACS statistics of *aeg*PNA-treated cells and thyclotide-treated cells. Cells were considered positive for cell uptake when the fluorescence was superior to the fluorescence observed for negative control (non-treated cells).

https://doi.org/10.1021/jacsau.3c00198
JACS Au 2023, 3, 1952−1964

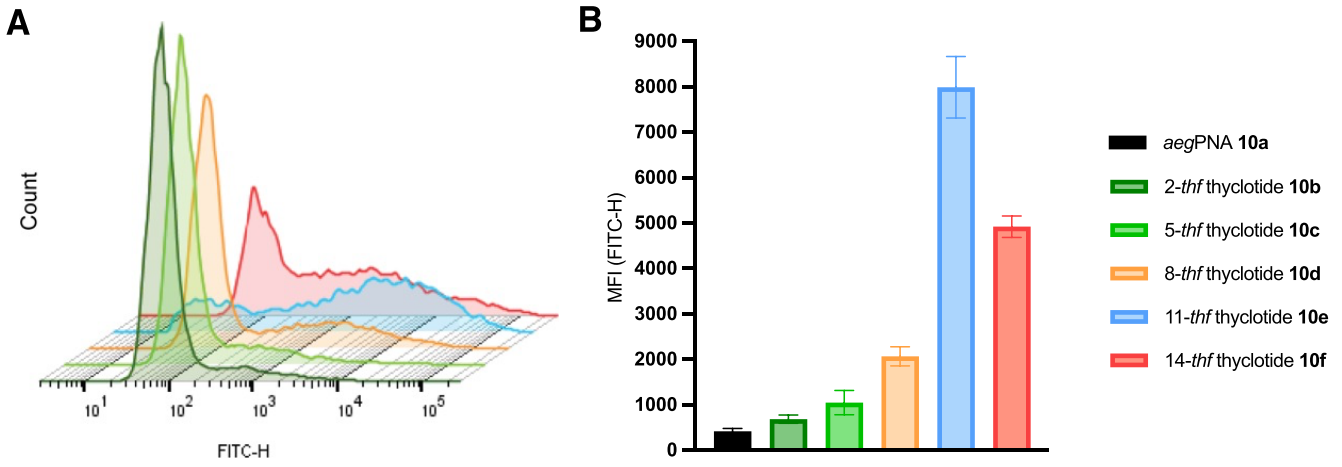

Figure 7. Relationship between the number of *thf* groups and cell uptake. (A) FACS of HCT116 cells treated with Fl-labeled thyclotides **10b** (dark green), **10c** (light green), **10d** (orange), **10e** (blue), or **10f** (red). (B) Comparisons of the MFI of HCT116 cells treated with Fl-labeled *aeg*PNA **10a** (black) and Fl-labeled thyclotides **10b** (dark green), **10c** (light green), **10d** (orange), **10e** (blue), and **10f** (red). $N = 3$.

Hydration of Thyclotide and *cp*PNA Determined by Osmotic Stressing

As thyclotide−DNA duplexes are more extensively hydrated than *cp*PNA−DNA duplexes in the solid state, we used osmotic stressing to evaluate their hydration in solution.[56,57] The dissociation of nucleic acid duplexes is influenced by changes in water activity. Addition of water-binding organic co-solutes, such as ethylene glycol and glycerol, will change the activity of water in an aqueous buffer and subsequently lower the melting temperature of oligonucleotide duplexes. Rozners and Moulder[57] established that the number of water molecules released upon the dissociation of oligonucleotide duplexes, Δn_w, can be calculated from melting temperatures at different levels of water activity. Thyclotide **9a** and *cp*PNA **9b** with identical seven-residue sequences were designed for these experiments since the melting temperatures for their binding to DNA and RNA fall within in the range of 40−70 °C in the presence of different organic co-solutes (Table 3 and Tables S13−S16). As shown in Table 3, the Δn_w values for oligonucleotide duplexes of thyclotide **9a** and *cp*PNA **9b** fall in a range of 0.47−1.16. These values are significantly lower than reported Δn_w values for DNA and RNA duplexes, which are 2−3 for DNA duplexes and 3−4 for RNA duplexes.[61] The results in Table 3 therefore suggest that oligonucleotide duplexes with thyclotide **9a** and *cp*PNA **9b** are less hydrated than duplexes where both strands are derived from DNA or RNA. Duplexes with RNA are typically more hydrated than those containing DNA.[57] Consistent with this trend, both thyclotide **9a**−RNA and *cp*PNA **9b**−RNA duplexes have Δn_w values that are slightly higher than the corresponding thyclotide **9a**−DNA and *cp*PNA **9b**−DNA duplexes (Table 3). It is also clear from the data that thyclotide **9a**−oligonucleotide duplexes have Δn_w values that are higher than the corresponding duplexes with *cp*PNA **9b** (Table 3). These results suggest that thyclotide **9a** is more hydrated than *cp*PNA **9b** when it binds to oligonucleotides, and this is consistent with the observations in the X-ray crystal structures.

Thyclotide Shows Good Cell Uptake

Thyclotides are polar molecules with a fairly rigid structure and good binding affinity and sequence specificity to complementary DNA and RNA. Some thyclotides with *thf* groups at every position are able to enter cells,[38] yet it seemed possible that a smaller number of *thf* modifications could still promote uptake into mammalian cells and subsequently target a miRNA inside the cell. Among the many different miRNAs, miR-21 is a 22-nucleotide oncogenic miRNA that regulates the expression of several proteins associated with many cancers.[58] Overexpression of miR-21 is a hallmark of many diseases.[59−61] To test for the cellular uptake of the different thyclotides, we synthesized the fluorescein (FI)-labeled *aeg*PNA **10a** and FI-labeled thyclotides **10b−10f** with a complementary nucleotide sequence to hsa-miR-21-5p (Figure 6A). The thyclotides were designed with a varying number of *thf* groups, ranging from 2 to 14, to directly determine the effects of differing numbers of *thf* groups on cell uptake. Initially, HCT116 cells were treated with the Fl-labeled *aeg*PNA **10a** or the Fl-labeled fully *thf*-modified thyclotide **10f** to establish the negative and positive controls, respectively. Using super-resolution microscopy, HCT116 cells treated with 2.5 μM **10a** clearly showed very weak fluorescence (Figure 6B and Figure S51), whereas cells treated with 2.5 μM **10f** show a strong green fluorescence, confirming that regular *aeg*PNAs are unable to efficiently enter the cells, while large amounts of the fully *thf*-modified thyclotide **10f** do enter the cells (Figure 6C and Figure S51). We then quantitated the difference in the uptake of Fl-labeled *aeg*PNA **10a** and Fl-labeled thyclotide **10f** by FACS. As shown in Figure 6D−F, 66% of HCT116 ($P < 0.0001$) treated with **10f** showed increased fluorescence compared with cells treated with **10a**, which displayed an uptake of only 13%. Even if a few cells were positive for the uptake of the *aeg*PNA, the mean fluorescence intensity (MFI) is significantly lower compared with the MFI of cells positive for thyclotide **10f** (12-fold increase; Figure 6G), showing that the number of molecules taken up per positive cell is much higher in the case of the thyclotide ($P < 0.0001$). Hence, the cellular uptake of thyclotide **10f** is considerably higher than that of *aeg*PNA **10a** in HCT116 cells ($P < 0.0001$).

Next, we investigated whether differing numbers of *thf* groups affected the cell uptake of thyclotides. Examining Fl-labeled thyclotides containing 2, 5, 8, 11, or 14 *thf* groups (**10b**, **10c**, **10d**, **10e**, and **10f**; Table S1 and Figure 6A), there is a clear trend that cellular uptake increases as more *thf* groups are incorporated into the thyclotide (Figure 7A,B). The increase in cell uptake is small for thyclotides containing 2, 5, or 8 *thf* groups compared with *aeg*PNA **10a**, but there is a very noticeable increase in cell uptake for thyclotide **10e** with 11 *thf* groups. Remarkably, the best thyclotide in terms of cell

https://doi.org/10.1021/jacsau.3c00198
JACS Au 2023, 3, 1952−1964

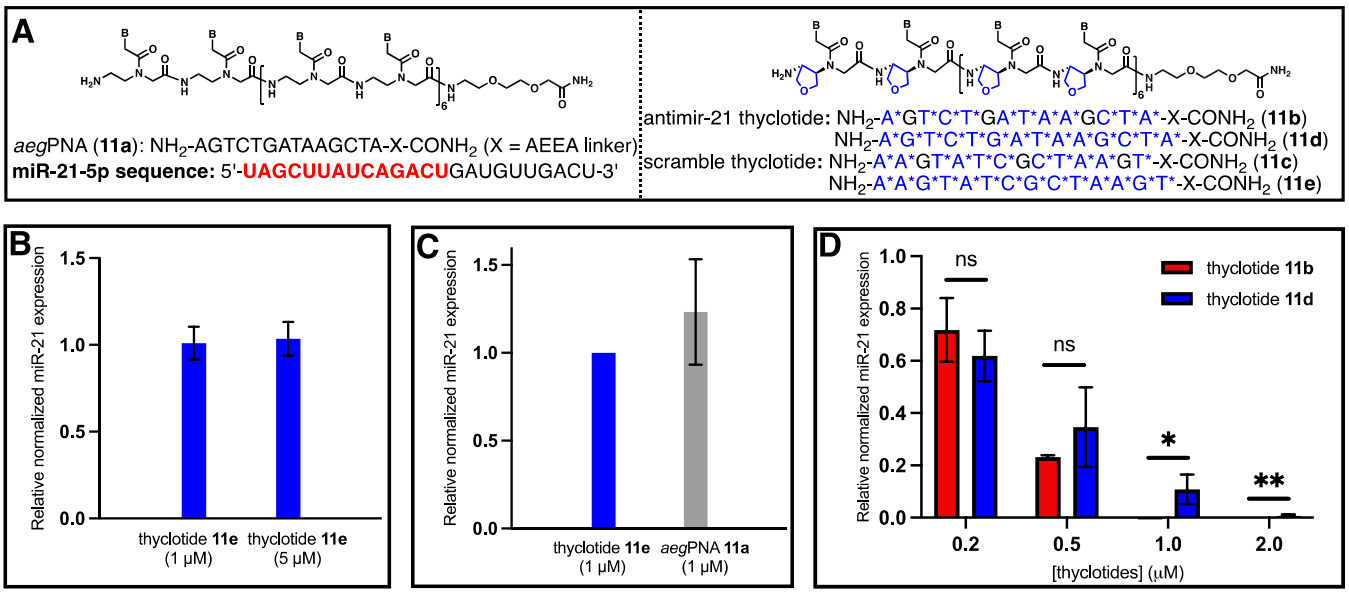

Figure 8. 11-*thf* and 14-*thf* thyclotides (**11b** and **11d**) inhibit miR-21. (A) AntimiR-21 *aeg*PNA **11a**, antimiR-21 thyclotides **11b** and **11d**, and scramble thyclotides **11c** and **11e** for RT-qPCR of miR-21. B* represents *thf* residue, and X represents 2-aminoethoxy-2-ethoxy acetic acid (AEEA linker). (B) RT-qPCR of miR-21 expression in HCT116 cells treated with 1 or 5 μM scramble thyclotide **11e**. miR-21 expression was normalized to non-treated cells. $N = 3$. (C) RT-qPCR of miR-21 expression in HCT116 cells treated with 1 μM antimiR-21 *aeg*PNA **11a**. miR-21 expression was normalized to scramble thyclotide **11e**-treated cells. $N = 3$. (D) RT-qPCR of miR-21 expression in HCT116 cells after treatment at varying concentrations of antimiR-21 thyclotide **11b** and **11d**. $N = 3$. Quantification was normalized to scramble thyclotide **11c** or **11e**. All RT-qPCRs used the combination of miR-25-5p and miR-93-5p as endogenous controls. The difference between miR-21 expressions after thyclotides **11b** and **11d** treatments was statistically significant using a one-tail paired *t*-test at 1 μM ($P = 0.0411$) and 2 μM ($P = 0.0033$).

uptake efficiency is not the fully modified-14-*thf* thyclotide **10f** but the 11 *thf*-thyclotide **10e** (Figure 7A,B). The enhanced uptake of the 11-*thf* thyclotide **10e** was confirmed by super-resolution microscopy (Figure S52). Clearly not every position in a thyclotide needs to be modified with *thf* to achieve optimal cell uptake, yet there is a critical number of *thf*'s that are needed. Typically, large molecules with molecular weights over 1000 Da have very poor cell permeability.[62] The thyclotides **10e** and **10f**, with molecule weights over 5000 Da, seem to be exceptions to the limits commonly seen with the cell uptake of sizable molecules.

Thyclotide Can Effectively Bind and Inhibit miR-21

Thyclotides **10e** and **10f** efficiently enter HCT116 cells but at somewhat different levels of efficiency. Next, we wanted to test if **10e** and **10f** can inhibit miR-21 in HCT116 cells and whether they have different potencies. To perform these experiments, we synthesized several controls. The first control sequence was the antimiR-21 *aeg*PNA **11a** (Figure 8A), which we expected to have no effect on miR-21 as HCT116 cells overexpress miR-21[63] and the fluorescein-labeled derivative of this *aeg*PNA was unable to enter these cells efficiently. The next control sequences are the scrambled thyclotides **11c** and **11e** (Figure 8A). The sequences of these control thyclotides are not complementary to miR-21 and therefore should not have any effect on miR-21 levels. HCT116 cells were treated with 1 or 5 μM **11e**, and expression of miR-21 was assessed by RT-qPCR compared with untreated cells. As shown in Figure 8B, the scrambled thyclotide **11e** was a good negative control as it did not induce any changes in miR-21 expression in HCT116 cells and did not exhibit any obvious cytotoxicity.[42] We then treated cells with antimiR-21 *aeg*PNA **11a** and measured miR-21 expression relative to cells treated with the scrambled sequences. As expected, **11a** was unable to inhibit miR-21 expression (Figure 8C). Gratifyingly, the antimiR-21 thyclotides **11b** and **11d** induce a strong dose-dependent response in miR-21 expression (Figure 8D). Thyclotides bind miR-21 strongly and act as steric blockers. Therefore, miR-21 is unable to be amplified by PCR, leading to an apparent decrease in expression levels by RT-qPCR after treating HCT116 cells with thyclotides **11b** and **11d**. The decrease in miR-21 expression reaches about 50% at a concentration of 500 nM **11d**, and total inhibition of miR-21 is obtained at 2 μM and higher (Figure 8D). Even though it has fewer *thf* groups, thyclotide **11b** is more potent than **11d**. At a concentration of 1 μM **11b**, there is a complete inhibition of miR-21 (Figure 8D). For thyclotide **11d** at a concentration of 1 μM, about 11% of miR-21 is still observed (Figure 8D). These results resemble the trend observed in the cell uptake experiments where the 11-*thf* thyclotide **10e** entered cells more effectively than 14-*thf* thyclotide **10f** (Figure 7). This is the first time we have shown that there is an optimal number of *thf* groups in a thyclotide to achieve maximal cell uptake and biological activity, and it is intriguing that the best activities are realized without placing *thf* groups at every position in the sequence.

CONCLUSIONS

Conformationally constrained *thf*-derived PNAs (thyclotides) exhibit remarkable binding properties and uptake by HCT116 cells. Incorporation of thyclotide monomers into PNAs enhances binding affinity and sequence specificity with DNA and RNA targets. CD experiments and an X-ray structure of thyclotide−DNA showed that the *thf* units rigidify the PNA backbone and preorganize PNAs into a right-hand helix. The polar *thf* units increase hydration compared with *cp*PNA, both in the solid state and in solution. This increased hydration may also contribute to the somewhat lower stability observed with thyclotide−oligonucleotide duplexes compared with the corre-

https://doi.org/10.1021/jacsau.3c00198
JACS Au 2023, 3, 1952−1964

sponding *cp*PNA duplexes. The increased binding properties and polarity of thyclotides seem to work in concert to promote the uptake of a thyclotide into HCT116 cells and to effectively inhibit the expression of miR-21. For the antimiR-21 sequence studied, there is an optimal number of *thf* groups in the thyclotide that results in the most potent biological activities in HCT116 cells. The sensitivity of cell uptake to the different numbers of *thf* groups in the sequence indicates that the chemical and physical properties of thyclotides can be finely tuned to maximize their biological activities. These unique properties will hopefully spark widespread use of thyclotides in a variety of applications across many areas of biomedical research.

METHODS

All materials and methods used including PNA/thyclotide synthesis, UV melting experiments, thermodynamic analysis, CD experiments, X-ray diffraction analysis, osmotic stressing experiments, and cell experiments are described in full detail in the Supporting Information.

Relative Polarities by HPLC

Thyclotide **3i**, *aeg*PNA **1a**, *mix*PNA **4a**, and *cp*PNA **2a** were dissolved in water to make 300 μM solutions. The four solutions were mixed in a 1:1:1:1 ratio, and the resulting solution was analyzed by HPLC (see page S4 for details).

Octanol Water Partition Coefficient (K_{ow}) Measurement

To the PNA solutions (**3i**, **1a**, **4a**, and **2a**) (300 μM in water, 200 μL) was added 200 μL of 1-octanol at room temperature (21.7 °C). The resulting solutions were vigorously shaken and sonicated for 1 h. Then, the resulting solutions were centrifuged to form solutions with two layers. The 1-octanol layer (100 μL) was diluted with DMSO (100 μL), and the resulting solution (100 μL) was injected into an Agilent (Santa Clara, CA) 1260 Series RP-HPLC using ultraviolet detection at 260 nm for analysis. The water layer (100 μL) was diluted with DMSO (100 μL), and the resulting solution (10 μL) was analyzed by HPLC (see page S4 for details). The K_{ow} values (Table S2) were determined as the formula $K_{ow} = A_o/(A_w \times 10)$, where A_o is the area under PNA peaks in the HPLC chromatogram for the 1-octanol layer, and A_w is the area under PNA peaks in the HPLC chromatogram for the water layer. Since 100 μL 1-octanol layer solution and 10 μL water solution were injected to HPLC for analysis, a factor of 10 was added to adjust the formula.

ASSOCIATED CONTENT

Supporting Information

The Supporting Information is available free of charge at https://pubs.acs.org/doi/10.1021/jacsau.3c00198.

Preparation of PNA and thyclotide oligomers; polarity experiments; UV melting experiments; thermodynamic analysis; circular dichroism (CD) experiments; preparation and purification of iodo-labeled thyclotide−DNA duplex; crystallization and X-ray diffraction analysis of the thyclotide **8**−DNA duplex; osmotic stressing experiments (hydration); cell experiments; HPLC chromatograms and mass spectra; NMR spectra; Figures S1−S113, Scheme S1, and Tables S1−S19 (PDF)

AUTHOR INFORMATION

Corresponding Authors

Istvan Botos − *Laboratory of Molecular Biology, National Institute of Diabetes and Digestive and Kidney Diseases, National Institutes of Health, Department of Health and Human Services, Bethesda, Maryland 20892, United States*; Email: botosi@niddk.nih.gov

Daniel H. Appella − *Synthetic Bioactive Molecules Section, Laboratory of Bioorganic Chemistry (LBC), National Institute of Diabetes and Digestive and Kidney Diseases (NIDDK), National Institutes of Health, Bethesda, Maryland 20892, United States*; orcid.org/0000-0001-7195-7764; Email: appellad@niddk.nih.gov

Authors

Hongchao Zheng − *Synthetic Bioactive Molecules Section, Laboratory of Bioorganic Chemistry (LBC), National Institute of Diabetes and Digestive and Kidney Diseases (NIDDK), National Institutes of Health, Bethesda, Maryland 20892, United States*

Victor Clausse − *Synthetic Bioactive Molecules Section, Laboratory of Bioorganic Chemistry (LBC), National Institute of Diabetes and Digestive and Kidney Diseases (NIDDK), National Institutes of Health, Bethesda, Maryland 20892, United States*

Harsha Amarasekara − *Synthetic Bioactive Molecules Section, Laboratory of Bioorganic Chemistry (LBC), National Institute of Diabetes and Digestive and Kidney Diseases (NIDDK), National Institutes of Health, Bethesda, Maryland 20892, United States*

Sharlyn J. Mazur − *Laboratory of Cell Biology, National Cancer Institute, National Institutes of Health, Department of Health and Human Services, Bethesda, Maryland 20892, United States*; orcid.org/0000-0002-6378-0791

Complete contact information is available at: https://pubs.acs.org/10.1021/jacsau.3c00198

Author Contributions

[#]H.Z. and V.C. contributed equally to this work.

Author Contributions

D.H.A., H.Z., and V.C. conceived and designed the experiments. H.Z. and H.A. prepared and purified thyclotide monomers and iodo-labeled thyclotide monomer. H.Z. prepared and purified all PNAs and thyclotides. H.Z. measured T_m's of PNA−DNA (RNA) duplexes and thyclotide−DNA (RNA) duplexes. H.Z. performed CD experiments on PNAs and thyclotides. H.Z. conducted the HPLC analyses and purifications of the thyclotide−DNA duplex. I.B. grew the single crystals and solved the crystal structure of the thyclotide−DNA duplex. S.J.M. and H.Z. analyzed the UV melting curves to obtain the thermodynamic parameters and Δn_w. V.C. performed all cell experiments. H.Z., V.C., and D.H.A. co-wrote the paper. D.H.A. supervised the entire study. All authors contributed to the final version of the paper.

Funding

This research was supported by the Intramural Research Program of NIDDK, NIH. Coordinates and structure factors of the thyclotide **8**−DNA duplex were deposited into the Protein Data Bank (PDB ID: 7UID).

Notes

The authors declare the following competing financial interest(s): Part of this work has been patented (Thyclotide. WO2021211786A1). Inventors: Daniel H. Appella, Hongchao Zheng, Harsha C. Amarasekara, Victor Clausse, George A. Kubi.

ACKNOWLEDGMENTS

We thank John Lloyd (NIDDK/NIH) for performing mass spectrometry and Robert O'Connor (NIDDK/NIH) for his assistance with NMR spectroscopy. We also would like to thank Francisco Moris, Nicolas Ríos-Lombardia, and Javier Sabin-

Gonzalez from the company Entrechem (Spain) for helping us to produce the chiral starting material (for the preparation of thyclotide monomers) *via* an enzymatic resolution.

ABBREVIATIONS

thf tetrahydrofuran
cp cyclopentane
PNA peptide nucleic acid

REFERENCES

(1) Uhlmann, E.; Peyman, A. Antisense oligonucleotides: a new therapeutic principle. *Chem. Rev.* **1990**, *90*, 543−584.
(2) Goodchild, J. Conjugates of oligonucleotides and modified oligonucleotides: a review of their synthesis and properties. *Bioconjugate Chem.* **1990**, *1*, 165−187.
(3) Sharma, V. K.; Sharma, R. K.; Singh, S. K. Antisense oligonucleotides: modifications and clinical trials. *Med. Chem. Commun.* **2014**, *5*, 1454−1471.
(4) Dhuri, K.; Bechtold, C.; Quijano, E.; Pham, H.; Gupta, A.; Vikram, A.; Bahal, R. Antisense oligonucleotides: an emerging area in drug discovery and development. *J. Clin. Med.* **2020**, *9*, 2004.
(5) Nielsen, P. E.; Egholm, M.; Berg, R. H.; Buchardt, O. Sequence-selective recognition of DNA by strand displacement with a thymine-substituted polyamide. *Science* **1991**, *254*, 1497−1500.
(6) Egholm, M.; Buchardt, O.; Nielsen, P. E.; Berg, R. H. Peptide nucleic acids (PNA). Oligonucleotide analogs with an achiral peptide backbone. *J. Am. Chem. Soc.* **1992**, *114*, 1895−1897.
(7) Nielsen, P. E. Peptide nucleic acid. A molecule with two identities. *Acc. Chem. Res.* **1999**, *32*, 624−630.
(8) Nielsen, P. E. Peptide nucleic acid: a versatile tool in genetic diagnostics and molecular biology. *Curr. Opin. Biotechnol.* **2001**, *12*, 16−20.
(9) Nielsen, P. E. PNA technology. *Mol. Biotechnol.* **2004**, *26*, 233−248.
(10) Egholm, M.; Nielsen, P. E.; Buchardt, O.; Berg, R. H. Recognition of guanine and adenine in DNA by cytosine and thymine containing peptide nucleic acids (PNA). *J. Am. Chem. Soc.* **1992**, *114*, 9677−9678.
(11) Egholm, M.; Buchardt, O.; Christensen, L.; Behrens, C.; Freier, S. M.; Driver, D. A.; Berg, R. H.; Kim, S. K.; Norden, B.; Nielsen, P. E. PNA hybridizes to complementary oligonucleotides obeying the Watson-Crick hydrogen-bonding rules. *Nature* **1993**, *365*, 566−568.
(12) Wittung, P.; Nielsen, P. E.; Buchardt, O.; Egholm, M.; Norden, B. DNA-like double helix formed by peptide nucleic acid. *Nature* **1994**, *368*, 561−563.
(13) Weiler, J.; Gausepohl, H.; Hauser, N.; Jensen, O. N.; Hoheisel, J. D. Hybridisation based DNA screening on peptide nucleic acid (PNA) oligomer arrays. *Nucleic Acids Res.* **1997**, *14*, 2792−2799.
(14) Ratilainen, T.; Homén, A.; Tuite, E.; Nielsen, P. E.; Nordén, B. Thermodynamic of sequence-specific binding of PNA to DNA. *Biochemistry* **2000**, *39*, 7781−7791.
(15) Pandey, V. N.; Upadhyay, A.; Chaubey, B. Prospects for antisense peptide nucleic acid (PNA) therapies for HIV. *Expert Opin. Biol. Ther.* **2009**, *9*, 975−989.
(16) Ray, A.; Nordén, B. Peptide nucleic acid (PNA): its medical and biotechnical application and promise for the future. *FASEB J.* **2000**, *14*, 1041−1060.
(17) Sardone, V.; Zhou, H.; Muntoni, F.; Ferlini, A.; Falzarano, M. S. Antisense oligonucleotide-based therapy for neuromuscular disease. *Molecules* **2017**, *22*, 563.
(18) Ghosal, A. Peptide nucleic acid antisense oligomers open an avenue for developing novel antibacterial molecules. *J. Infect. Dev. Ctries.* **2017**, *11*, 212−214.
(19) Dean, D. A. Peptide nucleic acids: versatile tools for gene therapy strategies. *Adv. Drug Delivery Rev.* **2000**, *44*, 81−95.
(20) Stender, H. PNA fish: an intelligent stain for rapid diagnosis of infectious diseases. *Expert. Rev. Mol. Diagn.* **2003**, *3*, 649−655.
(21) Roberto, G. Biological activity and delivery of peptide nucleic acid (PNA)-DNA chimeras for transcription factor decoy (TFD) pharmacotherapy. *Curr. Med. Chem.* **2004**, *11*, 1253−1263.
(22) Siddiquee, S.; Rovina, K.; Azriah, A. A review of peptide nucleic acid. *Adv. Tech. Biol. Med.* **2015**, *3*, 1000131.
(23) Wu, J.; Meng, Q.; Ren, H.; Wang, H.; Wu, J.; Wang, Q. Recent advances in peptide nucleic acid for cancer bionanotechnology. *Acta Pharmacol. Sin.* **2017**, *38*, 798−805.
(24) Perera, J. D. R.; Carufe, K. E. W.; Glazer, P. M. Peptide nucleic acids and their role in gene regulation and editing. *Biopolymers* **2021**, *112*, No. e23460.
(25) Nielsen, P. E. Addressing the challenges of cellular delivery and bioavailability of peptide nucleic acids (PNA). *Q. Rev. Biophys.* **2006**, *38*, 345−350.
(26) Corradini, R.; Sforza, S.; Tedeschi, T.; Totsingan, F.; Manicardi, A.; Marchelli, R. Peptidenucleic acids with a structurally biased backbone. Updated review and emerging challenges. *Curr. Top. Med. Chem.* **2011**, *11*, 1535−1554.
(27) Rozners, E. Recent advances in chemical modification of peptide nucleic acids. *J. Nucleic Acids* **2012**, *2012*, No. 518162.
(28) Sugiyama, T.; Kittaka, A. Chiral peptide nucleic acids with a substituent in the N-(2-aminoethy)glycine backbone. *Molecules* **2013**, *18*, 287−310.
(29) Moccia, M.; Adamo, M. F. A.; Saviano, M. Insights on chiral, backbone modified peptide nucleic acids: properties and biological activity. *Artif. DNA PNA XNA* **2014**, *5*, No. e1107176.
(30) Bordyagin, N.; Katkevics, M.; Kotikam, V.; Ryan, C. A.; Rozners, E. Chemical approaches to discover the full potential of peptide nucleic acids in biomedical applications. *Beilstein J. Org. Chem.* **2021**, *17*, 1641−1688.
(31) Suparpprom, C.; Vilaivan, T. Perspectives on conformationally constrained peptide nucleic acid (PNA): Insights into the structural design, properties and applications. *RSC Chem. Biol.* **2022**, *3*, 648−697.
(32) Shiraishi, T.; Nielsen, P. E. Peptide nucleic acid (PNA) cell penetrating peptide (CPP) conjugates as carriers for cellular delivery of antisense oligomers. *Artif. DNA PNA XNA* **2011**, *2*, 90−99.
(33) Gupta, A.; Bahal, R.; Gupta, M.; Glazer, P. M.; Saltzman, W. M. Nanotechnology for delivery of peptide nucleic acids (PNAs). *J. Controlled Release* **2016**, *240*, 302−311.
(34) Shiraishi, T.; Nielsen, P. E. Nanomolar cellular antisense acitivity of peptide nucleic acid (PNA) cholic acid ("umbrella)" and cholesterol conjugates delivered by cationic lipids. *Bioconjugate Chem.* **2012**, *23*, 196−202.
(35) Gasparello, J.; Manicardi, A.; Casnati, A.; Corradini, R.; Gambari, R.; Finotti, A.; Sansone, F. Efficient cell penetration and delivery of peptide nucleic acids by an argininocalix[4]arene. *Sci. Rep.* **2019**, *9*, 3036.
(36) Soudah, T.; Mogilevsky, M.; Karni, R.; Yavin, E. CLIP6-PNA-Peptide Conjugates: Non-Endosomal Delivery of Splice Switching Oligonucleotides. *Bioconjugate Chem.* **2017**, *28*, 3036−3042.
(37) Zheng, H.; Botos, I.; Clausse, V.; Nikolayevskiy, H.; Rastede, E. E.; Fouz, M. F.; Mazur, S. J.; Appella, D. H. Conformational constraints of cyclopentane peptide nucleic acids facilitate tunable binding to DNA. *Nucleic Acids Res.* **2021**, *49*, 713−725.
(38) Clausse, V.; Zheng, H.; Amarasekara, H.; Kruhlak, M.; Appella, D. H. Thyclotide, tetrahydrofuran-modified peptide nucleic acid that efficiently penetrate cells and inhibit microRNA-21. *Nucleic Acids Res.* **2022**, *50*, 10839−10856.
(39) Zhuang, B.; Ramanauskaite, G.; Koa, Z.; Wang, Z. Like dissolves like: A first-principles theory for predicting liquid miscibility and mixture dielectric constant. *Sci. Adv.* **2021**, *7*, No. eabe7275.
(40) Pitzer, K. S.; Donath, W. E. Conformations and strain energy of cyclopentane and its derivatives. *J. Am. Chem. Soc.* **1959**, *81*, 3213−3218.
(41) Ratilainen, T.; Norden, B. Thermodynamics of PNA interactions with DNA and RNA. *Methods Mol. Biol.* **2002**, *208*, 59−88.
(42) Fox, J. M.; Zhao, M.; Fink, M. J.; Kang, K. K.; Whitesides, G. M. The molecular origin of enthalpy/entropy compensation in biomolecular recognition. *Annu. Rev. Biophys.* **2018**, *47*, 223−250.

https://doi.org/10.1021/jacsau.3c00198
JACS Au 2023, 3, 1952−1964

(43) Sforza, S.; Haaima, G.; Marchelli, R.; Nielsen, P. E. Chiral peptide nucleic acids (PNAs): helix handedness and DNA recognition. *Eur. J. Org. Chem.* **1999**, 197−204.
(44) Kypr, J.; Kejnovská, I.; Renciuk, D.; Vorlícková, M. Circular dichroism and conformational polymorphism of DNA. *Nucleic Acids Res.* **2009**, *37*, 1713−1725.
(45) Lotan, N.; Yaron, A.; Berger, A. The stabilization of the α-helix in aqueous solution by hydrophobic side chain interaction. *Biopolymers* **1966**, *4*, 365−368.
(46) Monera, O. D.; Sereda, T. J.; Zhou, N. E.; Kay, C. M.; Hodges, R. S. Relationship of sidechain hydrophobicity and α-helical propensity on the stability of the single-stranded amphipathic α-helix. *J. Pept. Sci.* **1995**, *1*, 319−329.
(47) Taylor, G. L. Introduction to phasing. *Acta Crystallogr., Sect. D: Biol. Crystallogr.* **2010**, *66*, 325−338.
(48) Lavery, R.; Sklenar, H. Defining the structure of irregular nucleic acids: conventions and principles. *J. Biomol. Struct. Dyn.* **1998**, *6*, 63−91.
(49) Betts, L.; Jpsey, J. A.; Veal, J. M.; Joedan, S. R. A nucleic acid triplex formed by a peptide nucleic acid−DNA complex. *Science* **1995**, *270*, 1838−1841.
(50) Eriksson, M.; Nielsen, P. E. Solution structure of a peptide nucleic acid−DNA duplex. *Nat. Struct. Biol.* **1996**, *3*, 410−413.
(51) The, J. I.; Shivachev, B.; Rsapireddy, S.; Crawford, M. J.; Gil, R. R.; Du, S.; Madrid, M.; Ly, D. H. Crystal structure of chiral γPNA with complementary DNA strand: Insights into the stability and specificity of recognition and conformational preorganization. *J. Am. Chem. Soc.* **2010**, *132*, 10717−10727.
(52) Menchise, V.; De Simone, G.; Tedeschi, T.; Corradini, R.; Sforza, S.; Marchelli, R.; Capasso, D.; Saviano, M.; Pedone, C. Insights into peptide nucleic acid (PNA) structural features: The crystal structure of a D-lysine-based chiral PNA−DNA duplex. *Proc. Natl. Acad. Sci. U. S. A.* **2003**, *100*, 12021−12026.
(53) Bloomfield, V. A.; Crothers, D. M.; Tinoco, Jr, I. *Nucleic acids: structures, properties, and functions*. University Science Books 2000.
(54) Carugo, O.; Bordo, D. How many water molecules can be detected by protein crystallography? *Acta Crystallogr., Sect. D: Biol. Crystallogr.* **1999**, *55*, 479−483.
(55) Saenger, W.; Saenger, W. Water and nucleic acids. In *Principles of Nucleic Acid Structure*. Saenger, W. ed. Springer, 1984, pp. 368−384, DOI: 10.1007/978-1-4612-5190-3_17.
(56) Spink, C. H.; Chaires, J. B. Effects of Hydration, Ion Release, and Excluded Volume on the Melting of Triplex and Duplex DNA. *Biochemistry* **1999**, *38*, 496−508.
(57) Rozners, E.; Moulder, J. Hydration of Short DNA, RNA and 2'-OMe Oligonucleotides Determined by Osmotic Stressing. *Nucleic Acids Res.* **2004**, *32*, 248−254.
(58) Pfeffer, S. R.; Yang, C.; Pfeffe, L. M. The role of miR-21 in cancer. *Drug Dev. Res.* **2015**, *76*, 270−277.
(59) Kura, B.; Kalocayova, B.; Devaux, Y.; Bartekova, M. Potential clinical implications of miR-1 and miR-21 in heart disease and cardioprotection. *Int. J. Mol. Sci.* **2020**, *21*, 700.
(60) Sheedy, F. J. Turning 21: introduction of miR-21 as a key switch in the inflammatory response. *Front. Immunol.* **2015**, *6*, 19.
(61) Jenike, A. E.; Halushka, M. K. miR-21: a non-specific biomarker of all maladies. *Biomark. Res.* **2021**, *9*, 18.
(62) Matsson, P.; Kihlberg, J. How big is too big for cell permeability? *J. Med. Chem.* **2017**, *60*, 1662−1664.
(63) Ferraro, A.; Kontos, C. K.; Boni, T.; Bantounas, I.; Siakouli, D.; Kosmidou, V.; Spyridakis, Y.; Tsipras, I.; Zografos, G.; Pintzas, A. Epigenetic regulation of miR-21 in colorectal cancer. *Epigenetics* **2014**, *9*, 129−141.

https://doi.org/10.1021/jacsau.3c00198
JACS Au 2023, 3, 1952−1964